UCID-19342

Use of ICRH for Startup and Initial Heating of the TMX-U Central Cell

A. W. Molvik

S. Falabella

May 1982

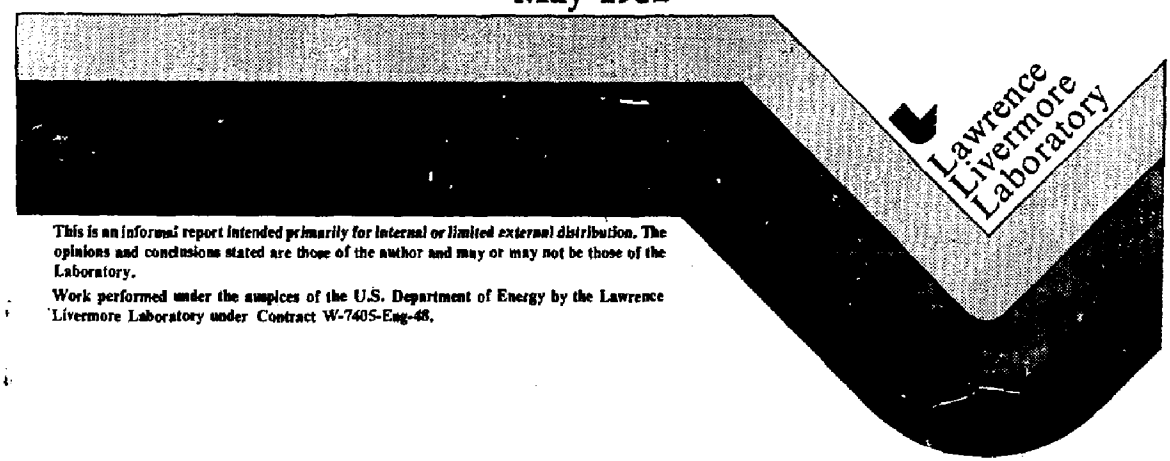

UCID--19342

DE82 016637

USE OF ICRH FOR STARTUP AND INITIAL HEATING OF THE TMX-UPGRADE CENTRAL CELL

A. W. Molvik and S. Falabella

Executive Summary

In this report, we evaluate ion cyclotron resonance heating (ICRH) and find it satisfactory for use in establishing the conditions necessary to form a thermal barrier in TMX-Upgrade (TMX-U). We discuss the constraints that must be satisfied in order to maintain a plasma, and outline a complete startup scenario that ends with the plasma at design parameters. The detailed discussions in this report concentrate on those parts of startup where ICRH is necessary. The ability of ICRH to couple power into a plasma at the fundamental ion cyclotron resonance, ω_{ci}, is determined from experiments with a half-turn loop antenna in the Phaedrus tandem mirror central cell. From these experiments, we get the empirical scaling that shows power deposited in the plasma is proportional to the plasma density.

Based on the theoretical interpretation of heating by evanescant fast waves, we expect, first, that the absorbed power will scale with the total number of ions in the resonance region. That is, the absorbed power should be proportional to the density, as observed, times the length of the zone times the plasma radius squared. The r^2 term provides for a factor of up to 9 times more power coupled into TMX-U than into the Phaedrus central cell. Such a scaling would be helpful, but is not required for TMX-U operation. Second, we expect that the scaling will hold only for evanescant (i.e., nonpropagating) waves. At higher densities, above $n \simeq 4 \times 10^{12}$ cm^{-3} in the TMX-U central cell, the fast wave at ω_{ci} begins to propagate. (The criterion for propagation is also proportional to nr^2.) We not only expect that a different scaling law will then be needed to describe the heating, but also expect that a propagating fast wave will not heat efficiently at ω_{ci}. This is because the left hand polarization, that is responsible for heating, is shielded by the plasma. At frequencies other than ω_{ci}, the left hand polarization is only partially shielded. For this reason, tokamaks use $2\omega_{ci}$ or minority heating at the fundamental resonance of the minority ion species, as it is off of the fundamental resonance of the majority that determines the polarization of the wave.

We find that the required ICRH power, for densities below 10^{12} cm^{-3}, is 60 kW leaving the antenna. This amount of power is available on TMX-U, and is substantially less than is routinely coupled into the central cell of the Phaedrus Tandem Mirror. The function of the ICRH is to heat the central-cell ions in order to reduce the barrier filling rate by reducing the collisionality of passing ions from the central cell. Then, the available pump neutral beams can adequately deplete the trapped ions. This must be done before a thermal barrier can be formed. Before barrier formation, we depend on magnetic confinement alone with no electrostatic axial confinement to reduce the power requirements. The power available dictates that a thermal barrier be formed at densities near or below 10^{12} cm^{-3}, or collisional flow will limit the ion temperature to below 100 eV which is too cold. Since we expect adequate heating, based on results from Phaedrus, we propose a half-turn loop antenna, similar to that in Phaedrus, for the TMX-U central cell. A similar evaluation of heating by neutral beams showed that the ratio of hot to cold ion densities must exceed fifteen during the startup period. This requires charge exchange lifetimes of ~20 ms for the hot ions, or higher neutral-beam current than is available. Furthermore, this increases the ratio of the central-cell beta to the plug beta to, or beyond, the MHD stability limit of ~2 shown in the TMX-U proposal; although higher stability limits are expected in practice because the anisotropic pressure in the central cell can preferentially weight regions of good curvature. We conclude that these factors make neutral-beam heating less attractive than ICRH during the initial phase of startup, before barrier formation.

After thermal barrier formation, we can continue the buildup to design level while maintaining the thermal barrier. Above a density of 10^{12} cm^{-3}, with the improved confinement from established thermal barriers, the power requirements are reduced to a level where neutral beams or a second ICRH system operating at the second or higher harmonics with a total power of 500 to 1000 kW, can complete heating the central-cell plasma to near the design parameters.

Introduction

This report discusses the proposed use of the ion cyclotron resonance heating, ICRH, for heating the central-cell ions in TMX-U[1] to assist in the startup of thermal barriers. Central-cell ion heating is required during startup and during equilibrium operation for several reasons: to decrease the collisional filling rate of the thermal barrier by central-cell ions passing into the plugs — which forms the subject of this report, as well as to study axial and radial confinement as a function of the central-cell ion temperature, and to study MHD stability as a function of the central-cell beta. ICRH has been demonstrated in the central cell and the end plugs of the Phaedrus tandem mirror.[2,3] During startup at low densities, ICRH at the fundamental ion cyclotron resonance ω_{ci} can more efficiently heat the bulk of the ion energy distribution, than can neutral beams. This will be discussed in Section 3. During equilibrium operation, either neutral-beam heating or ICRH at $2\omega_{ci}$ or higher harmonics should be satisfactory.

A number of constraints must be satisfied at all times during operation in order for the plasma to be maintained and a thermal barrier formed[4]:

1. Particle balance for each species in every region. The plug of a thermal-barrier tandem mirror can contain several species.
2. Power balance for each species in every region.
3. MHD stability.
4. Hot-ion microstability.
5. Hot-electron microstability.
6. Slow buildup of density in order to satisfy the hot-electron power balance. This is a subset of 2.
7. Thermal-barrier filling rates within the capability of the barrier pumping system.
8. Low gas influx on the plasma boundary. At the gas box, this must be the minimum required by the particle balance in order to obtain a favorable power balance and reduce barrier filling. Elsewhere, zero gas input is desirable.
9. Hot-electron fueling. This is a subset of constraint 1.

Barrier pumpability motivated this study of ICRH. The ratio of the collisional filling rate to the pumping rate in the thermal barrier is proportional to $n_c\ T_{ic}^{-1.5}$. The central-cell ion temperature must therefore be increased by some means as the density is increased in order to limit the filling rate. The initial plan was to heat the central-cell ions with neutral beams,[1] but then several constraints appeared difficult to satisfy. Startup at densities below $10^{12}\ cm^{-3}$ appears necessary to satisfy the hot-electron power balance. At such densities, neutral-beam heating is less efficient than ICRH for three reasons:

- The neutral beams heat the cold ions by collisions. At low densities, the hot density must greatly exceed the cold density in order to transfer sufficient power. This requires that the hot-ion lifetime against charge exchange be long and, therefore, that the surrounding gas pressure be low. Fundamental ion cyclotron heating, on the other hand, directly heats the bulk ions, as will be discussed.
- With neutral-beam heating, the central-cell beta will be dominated by the hot-ion component, and MHD stability appears to be marginal; although certain angular distributions may be stable.
- ICRH removes the gas influx that accompanies neutral beams; although tokamak studies have found increased impurity influx both with ICRH[5] and neutral beams.[5,6]

We are assuming the following startup scenario (described more fully in memos[7]): The thermal barriers are formed at a density of less than $10^{12}\ cm^{-3}$, then the plasma is gradually built-up to design parameters while maintaining the thermal barriers. In order to accomplish this, we

1. Turn on the startup guns at zero time to get an initial plasma of density less than $10^{12}\ cm^{-3}$.
2. Turn on sloshing-ion neutral beams to give enough plug beta for MHD stability, and turn on the central-cell ICRH to begin heating the ions to low enough collisionality for barrier pumping.
3. Turn on gas boxes to fuel the plasma (about simultaneously with the turn off of the startup guns).
4. Turn on ECRH while the plug density is below $10^{12}\ cm^{-3}$ to begin heating mirror-confined electrons and to protect the low-density plasma from being destroyed by impinging gas.
5. Turn on the pump beams when the plasma parameters for thermal barrier formation are within one pumping time of being established.

Once the barrier is established, the axial confinement of central-cell ions will switch from magnetic mirror to electrostatic confinement. This reduces the heating requirements for the ions, so the ICRH power can be programmed downwards. The density will increase to design level over an approximately 20-ms period, determined primarily by how fast the ECRH can heat the mirror-confined electrons, while maintaining the thermal barrier. The buildup rate could also be limited to somewhat below $10^{15}\ cm^{-3}\ s^{-1}$ by

the heating rate of central-cell ions with ICRH. The startup scenario will not be discussed in further detail in this report except for those areas that are crucial to evaluating the need for ICRH and the requirements on the ICRH system.

Two acronymns are frequently used for ion cyclotron heating. ICRF is the more general term and refers to the ion cyclotron range of frequencies. ICRF includes frequencies below the cyclotron frequency such as the slow wave as well as the second and higher harmonic frequencies that are beginning to be used.[8,9] For start-up of TMX-U, we plan to use the fundamental cyclotron frequency; therefore we are using the alternative acronymn ICRH that stands for ion cyclotron resonance heating.

This paper is divided into three sections. The first discusses the data base for ICRH in tandem mirrors—the experiments in Phaedrus. The second discusses the applicability of these results to TMX-U, and outlines the rf system requirements. In the third we discuss the power balance for central-cell ions both before and after a thermal barrier is formed in order to calculate the power required from the ICRH transmitter.

1. Propagation and Heating Measured in Phaedrus

Experiments with ICRF heating of central-cell ions began in TMX.[10] We solved several technical problems, but shut down TMX to begin TMX-U construction before the solutions could be tested. The transmitter was then sent on loan to the University of Wisconsin, Madison, where the central-cell heating experiments continued in collaboration with the Phaedrus Tandem Mirror Group in the Department of Nuclear Engineering. The results of these experiments are discussed in this section of the report, and will be reported in greater detail elsewhere.[3]

Phaedrus[11,12] uses ICRH for central-cell and plug heating. The axial positions of the antennas are shown in Fig. 1. All the antennas are located off the midplanes of their respective cells. The plug antennas[2] are straight rods parallel to the major diameter of the elliptical plasma fan, and are equivalent to half-turn loops. The central-cell antennas[3] are also half-turn loops (see Fig. 2). Two antennas are available in the central cell, but only one is used at a time. The first, with which we got almost all the data shown in this report, is shown in Fig. 2(a). It is a 7-cm wide copper strap, shielded from plasma bombardment by a limiter on either side. The limiters are separated axially from the antenna by 2.5 cm and extend 2.5 cm inside the antenna radius of 25 cm. The limiters are grounded and supported from their centers by a horizontal rod. The second antenna is similar [Fig. 2(b)], but is protected from plasma bombardment and is electrostatically shielded by a Faraday shield that blocks any line of sight to the plasma. This antenna had a lower Q, 60 versus 160, and a lower heating efficiency of about half that of the limiter shielded antenna. We attribute this lower efficiency to image currents in the shield that dissipate power. These lead to a lower Q and reduce the effective antenna current, thereby reducing the radiated power.[3]

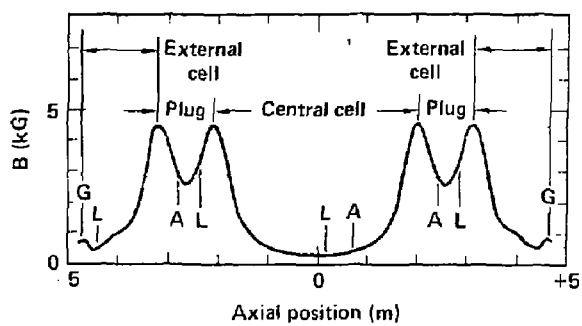

Figure 1. The axial magnetic field profile of the Phaedrus tandem mirror is shown after the plasma guns have been turned off and the current reduced in the surrrounding coils. We indicate the axial positions of (A) ICRH antennas, (L) diamagnetic loops, and (G) plasma guns near the end walls.

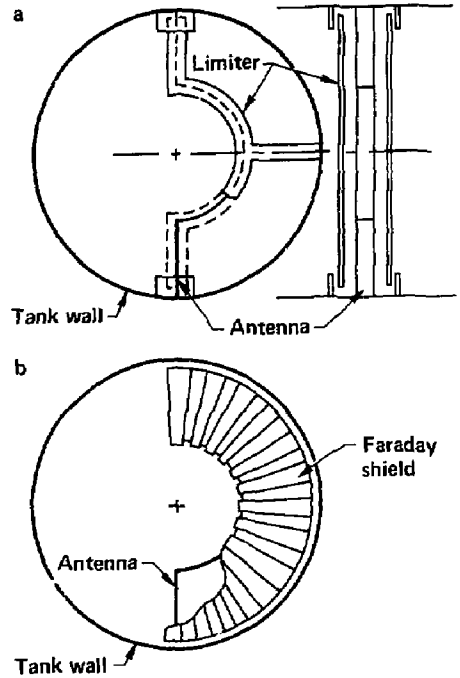

Figure 2. Half turn loops are used as ICRH antennas in the Phaedrus central cell (a) A bare copper antenna is shielded by limiters from plasma bombardment. (b) A Faraday shield, that blocks lines of sight from the plasma, reduces electrostatic coupling to the plasma as well as eliminating plasma bombardment of the antenna.

The transmitter used was on loan from TMX and has been described previously.[10] A block diagram, Fig. 3, shows the system as used on Phaedrus. The frequency is determined by an oscillator tuned to the resonant frequency of the non-variable impedance matching capacitors in parallel with the antenna. We connect an appropriate number of these capacitors to give the frequency range we want. The grid circuit of the final amplifier tube and the band pass filters on diagnostics such as the rf current and voltage are the only other rf circuits that must be tuned to resonance. Gating on the oscillator turns on the transmitter. The oscillator output is amplified to about 1 kW by a broadband amplifier that drives the grid of the final amplifier. With a capacitor bank charged to a maximum of 17 kV, a maximum power of 200 kW was delivered to the antenna. Losses in the antenna and matching capacitor dissipated 30% of the power, leaving up to 140 kW to be coupled into the Phaedrus central-cell plasma. The location of the cyclotron resonance is determined by the magnetic field strength in the central cell.

The heating in Phaedrus is interpreted as a damping of an evanescent fast wave at the fundamental ion cyclotron frequency.[2,3] This fits the data better in three main areas[2] than did an earlier interpretation in terms of a propagating slow wave. First the radiation resistance is proportional to rather than independent of the plasma density as predicted and observed for a slow wave in the C Stellarator.[13] Second, the radiation resistance was observed to be 0.14 Ω; rather than the 0.03 Ω expected for a slow wave. Third, the radiation resistance peaked for a resonance near the antenna rather than near the midplane. A slow wave propagates along the magnetic field at any plasma density, but a fast wave propagates mostly across the magnetic field and requires the order of one Alfvén wavelength across the plasma in order to propagate. More exactly, the condition for fast wave propagation is that[14]

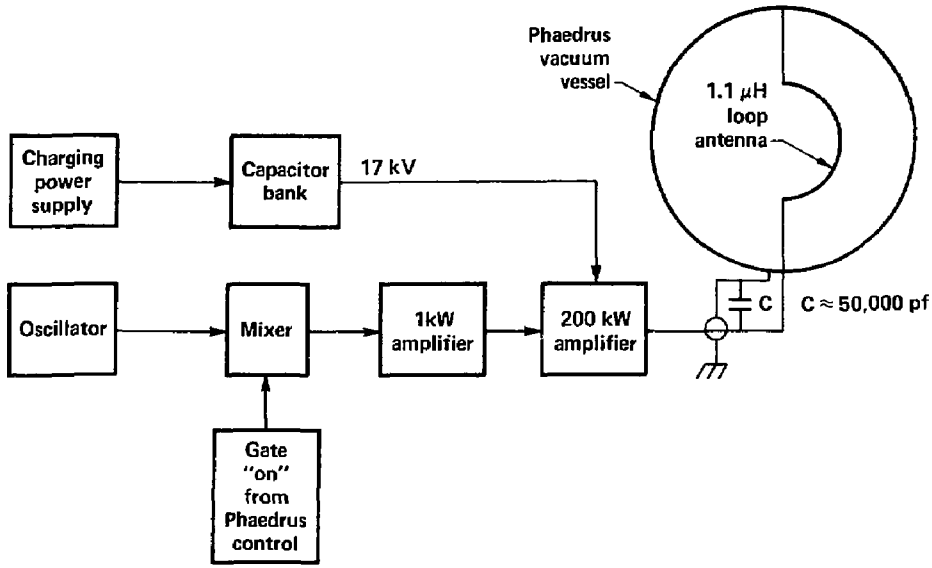

Figure 3. The ICRH system block diagram.

$$n(\mathrm{cm}^{-3})\, a^2(\mathrm{cm}) > 5 \times 10^{15} \frac{m_i}{m_H} \left(\frac{\omega_{ci}}{\omega}\right)^2 \tag{1}$$

for an m = 0 wave. The coefficient is reduced to 2×10^{15} for an m = 1 wave, which is expected to be the dominant mode from a half-turn antenna. Fast-wave propagation at the fundamental is therefore not expected in plasma of 8-cm radius in Phaedrus unless the density exceeds $3 \times 10^{13}\ \mathrm{cm}^{-3}$. All the data shown is for $n < 10^{13}\ \mathrm{cm}^{-3}$; hence a fast wave must be evanescent. In this report we are letting the plasma density in the TMX-U central cell have a parabolic profile that goes to zero at the limiter radius of 34 cm. This leads to fast-wave propagation above $n = 4 \times 10^{12}\ \mathrm{cm}^{-3}$ at the fundamental, and above $n = 10^{12}\ \mathrm{cm}^{-3}$ at $2\omega_{ci}$, where we have multiplied a^2 by $\kappa_2 = 0.5$ from Appendix A. We expect the results from Phaedrus to extrapolate to TMX-U only as long as the density is below the fast-wave propagation threshold. This density is sufficient for the initial phases of startup, before thermal barrier formation. This will be discussed further in Section 3.

The power absorbed in the central cell of Phaedrus, measured from the rate of rise of the diamagnetism, scaled proportionally to the density as shown in Fig. 4. The density was varied by gas puffing and by varying the central-cell magnetic field. This changes both the location and length of the resonance zones, which is expected to affect heating. To allow comparing data with the same magnetic geometry, points at the same magnetic field, with and without gas puffing, are connected by lines. These lines have slopes in the range of $n^{0.5}$ to n^2, all of which average to an approximately linear slope. The complete set of points is fit by the line $P(w) = 6 \times 10^{-9}\, n(\mathrm{cm}^{-3})$. In analyzing other sets of data, McVey plotted curves of power versus density[3] that can be fit by the lines $P(w) = 6000[V_B(kV)/6]^{1.4} + 3.3 \times 10^{-9}\, n(\mathrm{cm}^{-3})$, where V_B is the voltage of the energy storage capacitor bank. Note that the second scaling agrees with the first at the maximum density of $n = 10^{13}\ \mathrm{cm}^{-3}$ and maximum voltage $V_B = 17$ kV. At lower densities, the first scaling gives a lower, more conservative prediction. In Section 3, we will use the first scaling to estimate the power available on TMX-U, subject to the caveats discussed below.

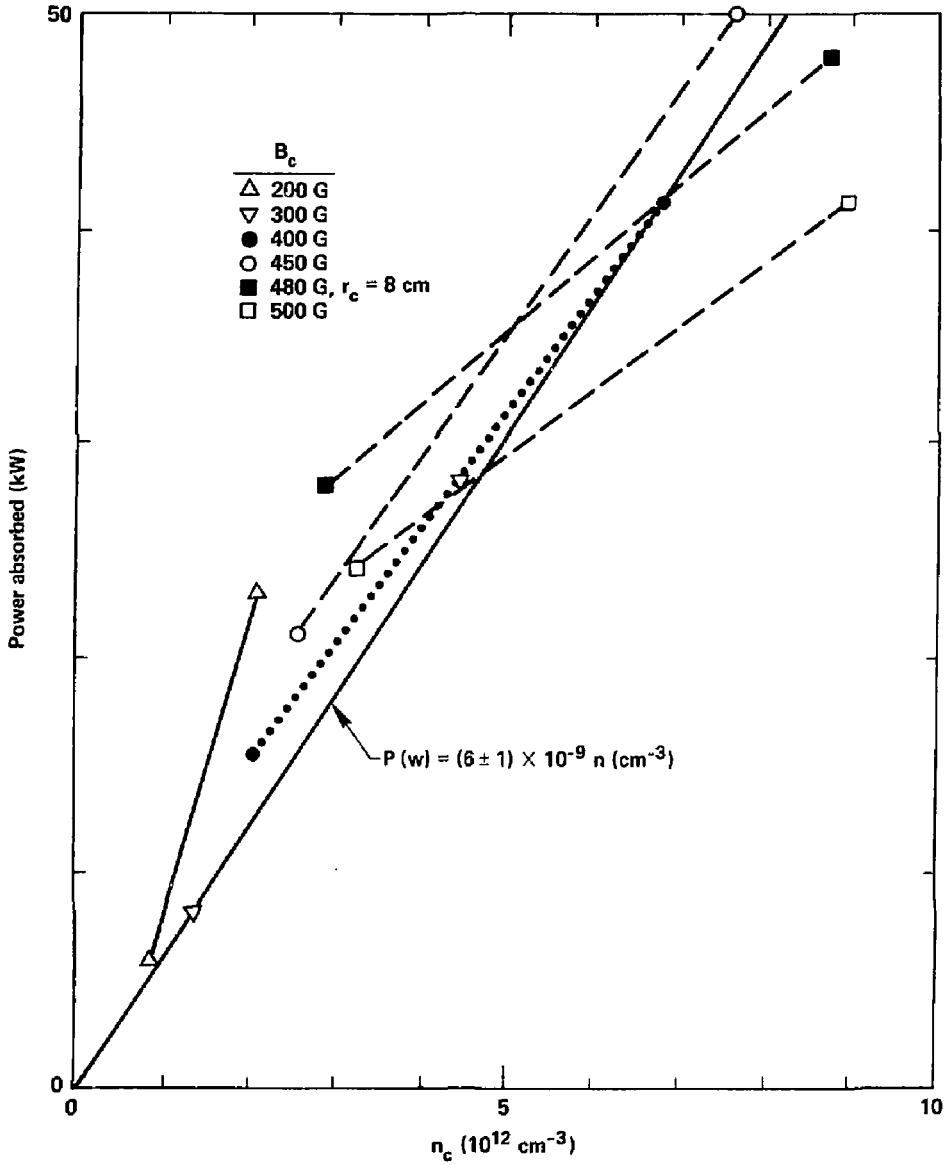

Figure 4. The ICRH power absorbed by the plasma is measured from the rate of rise of the diamagnetism in the Phaedrus central cell. The effects on the diamagnetic loop sensitivity and the plasma volume of varying the angular distribution of ions with B are not included.

The scaling of power versus density in Fig. 4 gives a lower limit to ion heating because an impedance mismatch between the transmitter and the antenna resulted in the transmitter output current saturating. The antenna impedance (Fig. 5) was lower than the transmitter impedance of 500 ohms for all the higher density data in the previous figures. This resulted in saturation of the rf current output of the tetrode amplifier when the antenna impedance was below about 200 ohms. Only for the pair of points at 200 G was the transmitter not saturated for either point. These points are closer to fitting n^2 than n. Higher power coupling can be expected on TMX-U if the antenna impedance is closely matched to that of the transmitter to eliminate its saturation. But, to be conservative, we will not count on this better coupling in estimating the power available.

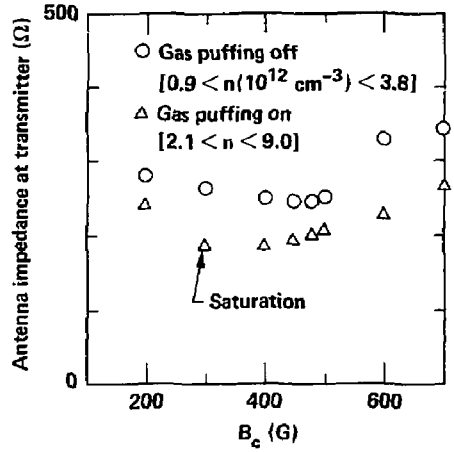

Figure 5. The transmitter output saturates at higher plasma density because the antenna impedance drops substantially below the output impedance of the transmitter.

When the plasma density is sustained by gas puffing, power is lost by charge exchange. For each ionization event occurring on a given flux tube, a certain number of charge exchange events also occur. The power scaling from Fig. 4 needs to be divided by f_i, the ratio of the cross-section for ionization by ion and electron impact to the total cross-section, including ionization plus charge exchange, in order to correct for the power lost by charge exchange and obtain the total ICRH power coupled into the plasma. In Fig. 6(a), the ratio of f_x, the complement of f_i, to f_i, is shown for protons incident on hydrogen atoms. The reaction rates σv are averaged over a Maxwellian energy distribution.[15] For average ion energies of 40 to 200 eV with ICRH in the Phaedrus central cell, the f_i was about 0.4. We use this fixed value in estimating the power coupled to the Phaedrus central-cell plasma to be

$$P(w) = 1.5 \times 10^{-8}\, n(cm^{-3}) \qquad (2)$$

McVey points out that above ~200 eV, charge exchange of protons on molecular hydrogen becomes significant, substantially increasing the loss of ions near the boundary,[3] as shown in Fig. 6(b).[15] For the results incorporated in Eq. 2, the assumption of proton charge exchange on a uniform density of hydrogen atoms is accurate. (Appendix A discusses this further.)

Boundary, or halo, heating is another sink for power in addition to charge exchange. If the particles in the boundary plasma have short lifetimes, most of the power that they absorb will not show up in the stored energy of the plasma column as measured by the diamagnetic loops. We inferred boundary heating

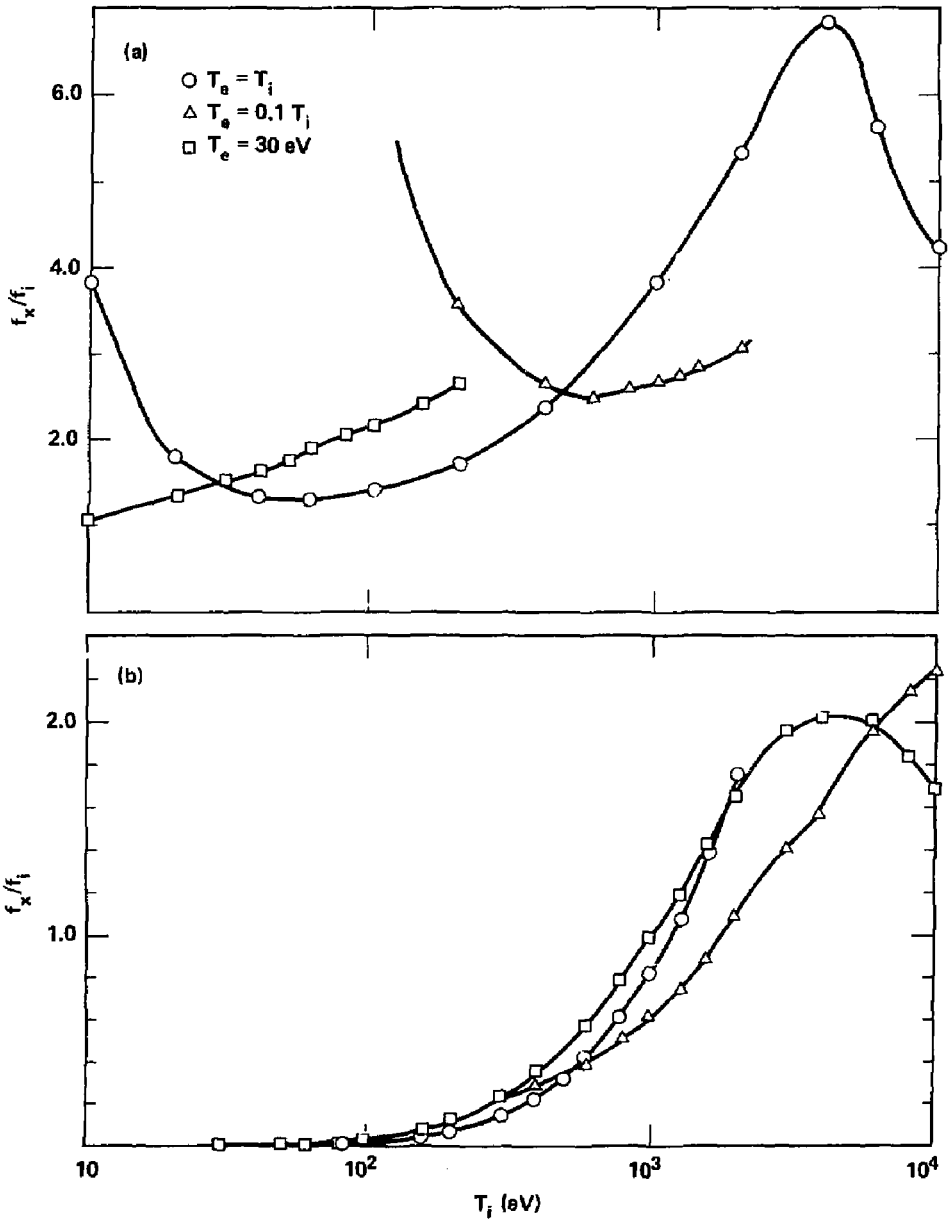

Figure 6. The ratio of the fraction of gas that charge-exchanges to that which is ionizd is shown versus the ion temperature. The ratio depends on the electron temperature. Results are shown for $T_e = T_i$, $T_e = 0.1T_i$, and $T_e = 30$ eV. The results shown average σv over a Maxwellian[14] ion distribution, *but do not include gas penetration effects.*[A1] The interaction of protons is shown with (a) hydrogen atoms and (b) hydrogen molecules.

from data gathered during a radial scan of a magnetic loop probe from the axis to the wall, Fig. 7(a) and 7(b). This probe measured the local change in the axial magnetic field caused by diamagnetic currents. The results do not show the expected reversal of ΔB outside of the diamagnetic current until a radius of 50 cm. Data at 24 cm, outside of 19-cm radius limiters, shows no reversal of ΔB. We conclude that this must be because of finite plasma pressure even outside the limiters. (The data in Fig. 7 were taken with the Faraday shielded antenna. The probe was located between the antenna and the limiter. All other data in this report were taken with the limiter shielded antenna.) We estimate the power drain due to edge heating as follows. We calculate an ion flow time into the limiter near the midplane (Fig. 1) of $\sim 10\ \mu s$, a plasma volume of $0.5\ m^3$, which with the boundary plasma energy of $0.28\ J\ m^{-3}$ gives a power drain of about 14 kW. Even with the large uncertainty in this power determination, boundary heating is unlikely to substantially reduce the core heating efficiency, but it could have other effects. For example, similar effects are probably responsible for the large increase in impurity radiation observed in the Princton Large Torus (PLT) with ICRH.[5] When better understood and controlled, boundary heating should become a valuable technique for providing a large-radius plasma halo capable of dissociating incident molecules far enough from the plasma that much less than the usual 50% of Franck-Condons reach the plasma core. Mirror experiments that have a large ratio of wall radius to plasma radius should provide a good geometry for such control of edge heating with minimal impurity influx.

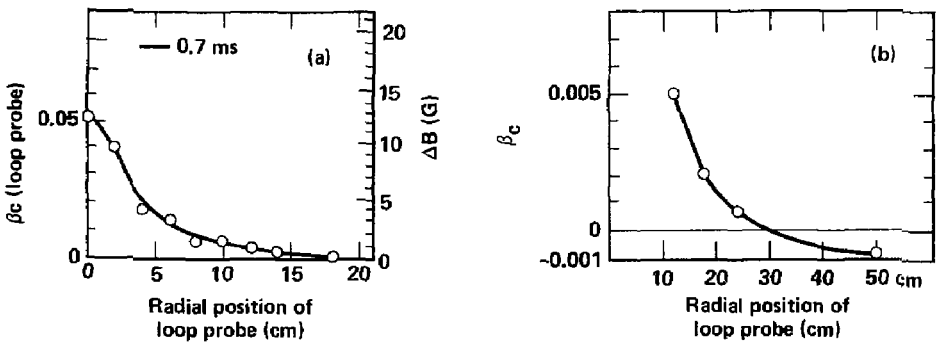

Figure 7. The change in the magnetic field of Phaedrus due to plasma diamagnetism, and the inferred beta, are plotted versus the radial position of the magnetic loop probe in (a). The line is described by the equation:

$$\beta_c = 0.0345\ \exp[-(r/3)^2] + 0.0165\ \exp[-(r/10)^2] \text{ for 0.7 ms data}$$

In (b), the scale is expanded to show the diamagnetic field near and outside the limiter that is at r = 19 cm.

The heating efficiency is determined from the ratio of the power coupled into the plasma (determined from diamagnetism and shown by the open data points in Fig. 8) to the rf power measured leaving the antenna. The efficiency for a constant 220-cm length plasma peaks at 40 to 80%, depending on the density, for a cyclotron resonance near the midplane. The solid data points are corrected for atomic charge exchange losses on the fraction of the density due to gas puffing, rather than gun injection. If we were to assume that the plasma is confined between the cyclotron resonance points in a sloshing-ion distribution, then the volume and the $E_\parallel$ would be functions of the magnetic field. The fixed length approximation is appropriate with gas puffing, shown by square data points, where $n \simeq 1 \times 10^{13}\ cm^{-3}$ and $T_{ic} \simeq 140$ eV, for which $\tau_c/\tau_{ii} \simeq 2.6$. That is, the central-cell ion confinement time is a few ion-ion collision times; hence we expect the distribution to be reasonably isotropic as assumed in Fig. 8. Without gas puffing the density is lower, $n \simeq 3.5 \times 10^{12}\ cm^{-3}$, and the temperature is higher, $T_{ic} \simeq 220$ eV, for which $\tau_c/\tau_{ii} \simeq 1.2$. This data is shown by the open circles in Fig. 8. These ions can be expected to have a sloshing distribution, that will cause the volume to be a function of the location of the resonance.

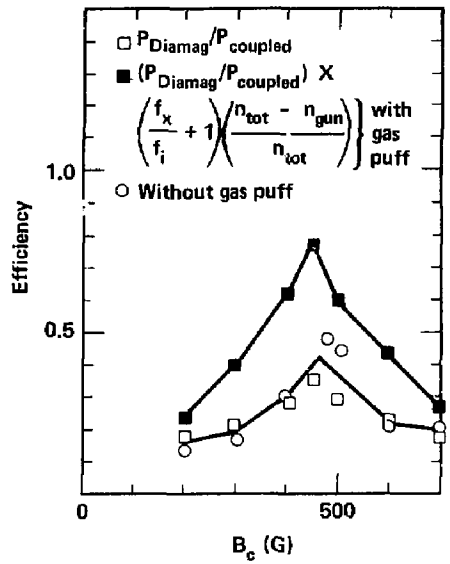

Figure 8. The ICRH heating efficiency in Phaedrus with data from Fig. 1-4, with and without the correction for charge-exchange from Fig. 1-6, is shown. The efficiency is defined as the ratio of the power absorbed in the plasma to that leaving the antenna.

Heating the bulk, rather than just the tail, of the ion energy distribution is required in order to reduce the collisional filling of the thermal barrier to a pumpable rate. Bulk heating is predicted theoretically for ICRH at the fundamental ion cyclotron frequency, ω_{ci}, where the heating rate is predicted to be proportional to the density and independent of the ion temperature.[14] A different result is predicted at $2\,\omega_{ci}$ where the heating rate is predicted to be proportional to the product of the ion density times the temperature[14] which will preferentially heat the high-energy tail of the ion distribution. These predictions are supported by two sets of measurements. Charge exchange measurements in a Phaedrus plug heated at ω_{ci} show the energy distribution perpendicular to the magnetic field to be Maxwellian over nearly two orders of magnitude in signal, Fig. 9.[16] (Tail heating was observed with $2\,\omega_{ci}$, also as expected.[11]) The second measurement is to determine T_{ip} from diamagnetism. This measurement is found to agree with T_{ip} from the charge exchange analyzer to within the experimental uncertainty of 40%.[17] We conclude that ω_{ci} heating will heat the bulk of the ions as required. At higher density and after the thermal barriers have been established , the collisional exchange of energy from a tail to the bulk will be rapid enough that either $2\,\omega_{ci}$ or neutral-beam heating will be satisfactory, as discussed at the end of Section 3.

2. rf Propagation and Heating Expected in TMX-U

We plan to use an antenna of approximately a half turn, located off the midplane in TMX-U at a magnetic field of 4 to 5 kG, as shown in Fig. 10. We select a half-turn over a full-turn antenna because the former was observed to heat five times more effectively in Phaedrus single-cell experiments.[2] The off-midplane location is selected because that location has worked effectively in Phaedrus[3] and will provide greater flexibility as is described next. We will use a Faraday-shielded antenna based on the TMX experience where the Q of a Faraday-shielded antenna was unaffected by gettering; whereas gettering was measured to decrease the Q of a limiter shielded antenna by a factor of at least five.[10] The heating with a Faraday-shielded antenna was less effective by a factor of two on Phaedrus, but we attribute some of the

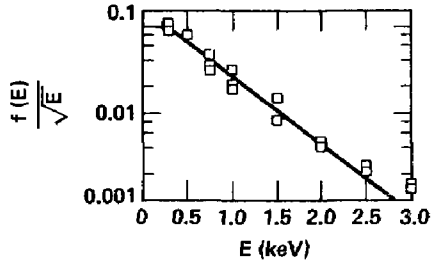

Figure 9. The ion energy distribution is measured in the west plug of Phaedrus with a charge-exchange analyzer during ICRH heating at ω_{ci}. The line is a Maxwellian distribution fit to the data. The fit is consistent with bulk heating.

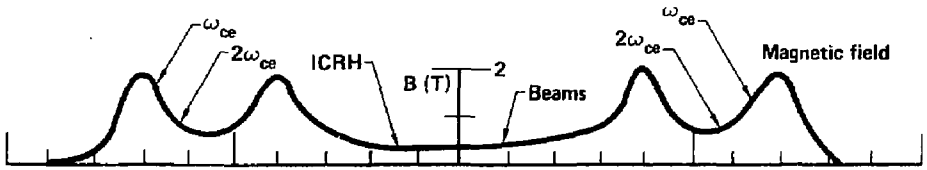

Figure 10. The TMX-U magnetic field strength along its axis is shown. An ICRH antenna will be located at z ≃ 1.3 m.

poorer performance to the saturation of the transmitter rf current. This prevented the antenna current from increasing to make up for the bucking effect of the image currents flowing in the shield.[3] We expect less than a factor of two reduction in heating, because of a Faraday shield in TMX-U, when the impedance of the antenna is closely matched to that of the transmitter. Other types of antennas, such as the Nagoya Type III[18] or an aperture antenna,[19] may prove superior and should be evaluated in future experiments.

Flexibility to explore different ICRF heating regimes in TMX-U is important in order to increase the probability of success in TMX-U, to provide a basis for comparison with the much more extensive theoretical and experimental data for ICRF heating in tokamaks,[8,20,21] and to provide a basis to extrapolate to MFTF-B and beyond. For this purpose, we need to provide capability in the following frequency ranges: 4 to 6 MHz to provide a fundamental resonance on the low-field side of the antenna, 6 to 9 MHz to provide a fundamental resonance on the high-field side of the antenna (i.e., towards the transition region), and 9 to 12 MHz to provide second harmonic heating in the central cell. This will allow studying, for example, the effects of the two-ion hybrid resonance which occurs between the cyclotron frequencies of the majority and minority ions.[8] This is important in understanding heating in tokamaks, where either ion or electron heating can dominate, depending on whether the wave is incident from the low- or high-field side of the hybrid layer respectively. This may be different in mirrors where the resonance surfaces are nearly perpendicular rather than nearly parallel to the magnetic field, and needs more study. Second and higher harmonic heating is important for three reasons:

- The fundamental fast wave is 100% right-hand polarized in an ideal model so will not heat ions; although nonideal effects such as impurities and slightly off-resonance frequencies may produce some left-hand polarization resulting in ion heating. Furthermore, mode conversion to a slow wave or Bernstein wave at a hybrid resonance could result in efficient heating.
- Higher harmonics will propagate at a lower density, and have higher-order radial eigenmodes as the density increases, thereby providing more uniform heating across the plasma cross-section, as discussed in the previous section. Heating of hydrogen plasmas at $2\,\omega_{ci}$ in PLT has shown higher than expected damping[8] as has third to fifth harmonic heating in the Elmo Bumpy Torus (EBT).[9]

- Varying the frequency will provide the capability of studying mode conversion or wave reflection effects at the ends of the central cell, as discussed in the next paragraph. Higher harmonic heating in the central cell is not expected to be useful during start-up of a thermal barrier, but it could be useful for maintaining the central-cell ion temperature during thermal barrier operation in TMX-U or MFTF-B.

The use of ICRH during startup at low plasma density forms the main topic of this report, and can be based on data from the Phaedrus tandem mirror. However, at densities exceeding 4×10^{12} cm^3 in the central cell of TMX-U, fast waves will propagate (see Eq. 1) giving an ion-heating regime that has not previously been observed in tandem mirrors. Experiments in tokamaks, including PLT, have found ICRF heating to be effective in both minority heating at ω_{ci}[8,20,21] and majority heating at $2\,\omega_{ci}$[8] regimes. Two criteria will determine whether propagating fast waves can heat effectively in mirrors. The first is the damping rate of the wave; if this is high enough for the wave to damp in one transit from the antenna to the end of the plasma cell, then the heating will be efficient. Results from both PLT[8] and EBT-S[9] indicate that the heating at $2\,\omega_{ci}$ and higher harmonics is much more efficient than predicted by theory,[22] but the consequences have not been evaluated for mirrors. If the damping rate is insufficient to absorb the wave energy in one transit, the heating can still be efficient if the wave reflects at the end of the mirror cell. In Eq. 1, both a^2 and ω_{ci} depend on the magnetic field strength, so for sufficiently low ω, the fast wave will not propagate to the mirror. The second criterion is whether the wave reflects at the ends of the fast wave propagation region. The heating will be more efficient if a standing wave, or cavity resonance, is established than if the wave continues to propagate by becoming evanescent or by mode converting. In the only related experiment that we are aware of, the fast wave was found to mode convert to a slow wave and continue propagating.[23] This particular result seems unlikely to hold universally because the fast wave propagation is a function of density, cross-sectional area and frequency; whereas the slow wave will propagate only below ω_{ci}, so that by sufficiently separating the propagation regions, mode conversion to a slow wave should be avoidable. Conversion to other modes may still happen.

The power coupling to the plasma in TMX-U is estimated to be at least as high as was observed in Phaedrus, Fig. 4. Theoretically,[24] the coupling is expected to be proportional to the number of ions in the resonance zone, which scales as $na^2(dz/dB)\,B$. If we evaluate these factors individually, we find the length of the resonance zone will be less at the midplane of TMX-U than in Phaedrus, but similar elsewhere. The central-cell radius is two to three times the $a = 8$ cm value of the Phaedrus central cell. Finally, as discussed earlier, the Faraday shield may reduce the coupling by as much as a factor of two. Including all these effects, we expect the power into the TMX-U plasma to be in the range of 0.5 to 4.5 times the power coupled into Phaedrus, with the upper limit more probable than the lower limit.

Startup of a thermal-barrier tandem mirror requires heating the entire plasma cross-section, particularly the core, to be sufficiently collisionless that the passing ions are not trapped in the barrier more rapidly than they can be pumped. Since ECRH, electron cyclotron resonance heating, is in many ways similar to ICRH, and since ECRH is well known to produce rings[25] rather than disks of hot electrons, we ask, why shouldn't ICRH produce ion rings? We argue that in the ECRH experiments to date, electron rings were to be expected. In fact, as well as we can determine from conversations with ECRH experimentalists, no experiments have been performed in the geometries shown in Fig. 11(b) or (c) that we expect to produce disks. In Fig. 11(a), we show the typical EBT electron ring producing geometry where a fundamental resonance, off the midplane, heats the entire plasma cross-section and supplies warm electrons to the second harmonic resonance which exists only off axis at the midplane. The second harmonic resonance surface is parallel to field lines, so provides a long correlation time for resonant electrons and results in efficient heating. It should, and does, produce rings in the vicinity of the second harmonic resonance. A central cell non-minimum-B region is shown in Fig. 11(b). In this case we place the fundamental and, if present, the second harmonic resonance, sufficiently far off the midplane that they cut across the entire plasma cross-section, even with finite beta. We then expect to produce a disk rather than a ring; however the heating efficiency may not be as high as in Fig. 11(a); because in Fig. 11(b), the mod-B surfaces normal to B produce short resonance regions. A third case, a minimum-B plug, is shown in Fig. 11(c). Here, as in the central cell, we expect to be able to obtain disks rather than rings by locating the resonances off the midplane. However, it is also necessary to restrict the plasma radius so that the resonance zone, if it closes at the midplane, is outside of the plasma. Otherwise the heating is equivalent to the EBT case of Fig. 11(a) and a ring can be expected. Finally, the pressure profile in the Phaedrus central cell, Fig. 7, showed that ion heating extended to the axis; if anything, peaking near the axis. We conclude that we can expect ICRH to heat the entire plasma cross section in TMX-U.

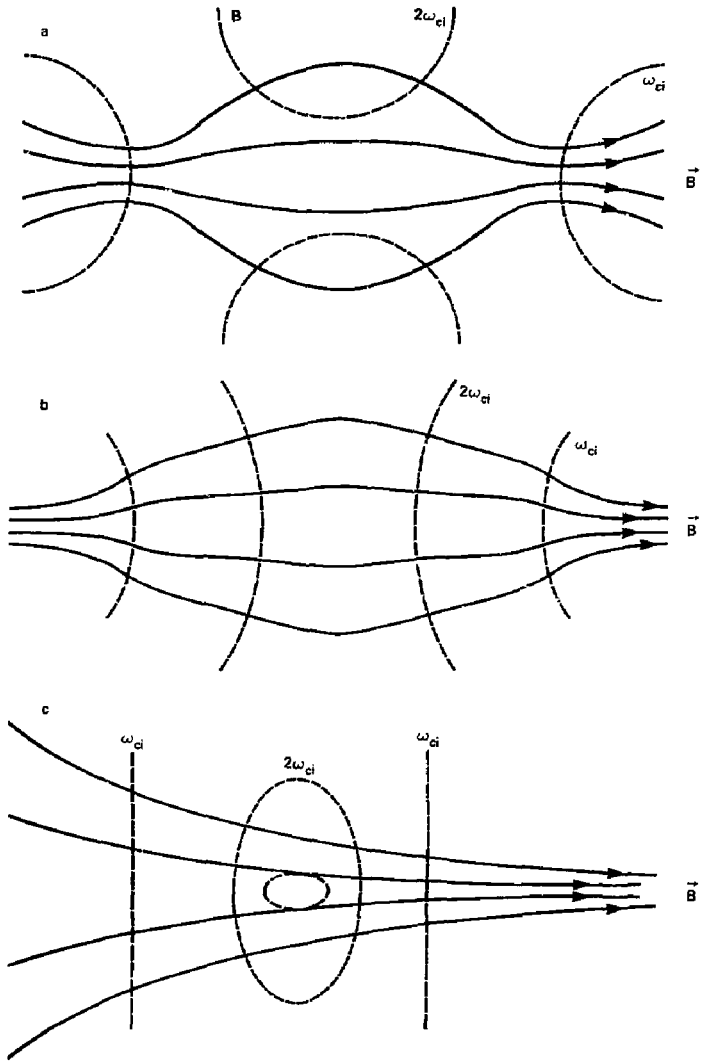

Figure 11. Magnetic field lines and constant Mod-B surfaces are shown for (a) an EBT-like configuration that has been shown to produce electron rings near the second harmonic resonance surface. (b) a simple mirror field, similar to the TMX-U central cell where the second harmonic, as well as the fundamental, resonance surfaces cover the entire plasma containing flux tube. Here, we expect to produce disks rather than rings of ions. (c) A minimum-B mirror, where by arranging the resonance surfaces as shown, and by excluding the plasma from larger radii where the mod-B surface becomes tangent to a flux surface, we expect a disk, rather than a ring. In TMX-U, where the radial well is very shallow, avoiding a ring should be easier than indicated in (c).

3. Particle and Power Balance for ions in the Central Cell of TMX-U

The ICRH power requirements are needed to specify the system requirements, and to compare with previous experiments to determine whether sufficient power can be coupled into the plasma. We determine the requirements by first determining the minimum ion temperature required for barrier pumpability, then determining the gas box fueling requirements in steady state and during buildup, and finally evaluating the axial, radial, drag, and charge exchange power losses. We do this for two cases: Magnetic confinement but no electrostatic confinement, which applies before the thermal barrier is formed; and Pastukhov confinement after the barrier is formed. In each case we will comput the power as a function of density needed to maintain a sufficiently high ion temperature for the barrier to be pumped. Figure 12 shows the barrier pumping requirement on the central-cell density and temperature scaled from the design parameters of $n_c = 1.7 \times 10^{13}$ and $T_{ic} = 900$ eV for a constant barrier collisional filling rate. The line shown is $(n_c/T_{ic}^{1.5}) \approx 6.3 \times 10^8$, giving an approximate value for the minimum temperature that is pumpable with the design level of 165 A of pump neutral beam per plug. In this section we will use Logan's nomenclature from the TMX-U Proposal, Appendix A2.[1] For example, we will refer to the bulk ion species in the central cell as the cold component. The second subscript c for cold will be generally omitted but is to be understood, except when the subscript "h," for hot ions, is specifically used. This will be when neutral beams or second harmonic ICRH, that heats a tail, are evaluated. As discussed earlier, the fundamental resonance heats the bulk of the distribution.

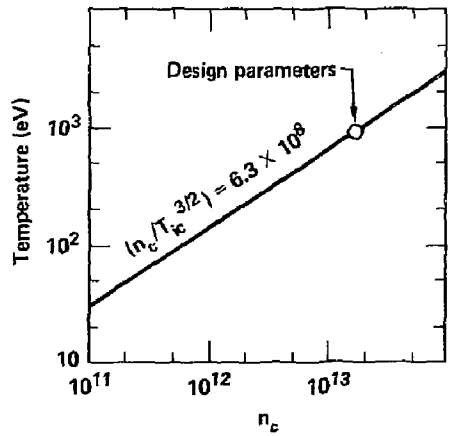

Figure 12. The minimum central-cell ion temperature in order to maintain a pumpable barrier in TMX-U is plotted versus density. This is scaled from the design parameters assuming collisional filling and neutral beam charge-exchange pumping of the barrier, with the incident beam current constant at the minimum adequate level.

The cold-ion particle balance determines the gas current required as a function of the ion density and temperature. It is given by

$$q\frac{dn_c\kappa_2 V}{dt} = \frac{f_i I_{gas}}{\Gamma} - \frac{qn_c\kappa_2 V}{\tau_{rad}} - \frac{qn_c{}^2 V}{n_c\tau_c}\left(\frac{\kappa_1 n\tau_1 + \kappa_2 n\tau_2}{n_c\tau_c}\right) \qquad (3)$$

This equation is discussed in detail in Appendix A. The gas feed requirements are shown in Fig. 13 for five cases: Curve A shows Eq. 3 with $dn/dt = 0$ for steady-state operation and $\Phi = 0$ before thermal barrier formation. Curves D and E are for the same conditions: a density buildup rate of $dn/dt = 10^{15}$ cm^{-3} s^{-1}

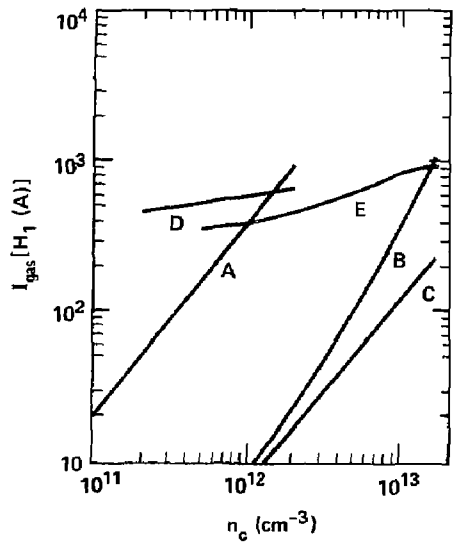

Figure 13. The gas current, in equivalent amperes of atoms, required to sustain the plasma at a pumpable temperature is shown versus the central cell density. The current injected by the gas boxes is expected to be within a factor of 2 of the values shown, which are calculated for $\Gamma = 2$ in Eq. A10. The ion temperature varies with density as in Fig. 12. Five curves are shown: A–C are for a steady-state density, curve A is without and curves B and C are with a thermal barrier of $\Phi/T_{ic} = 2.44$. Radial losses are included in curves A and B, but not in C. The nearly horizontal lines, curves D and E, are for a density buildup of $dn/dt = 10^{15}\ cm^{-3}\ s^{-1}$ with no losses. Before thermal barrier formation, we let $T_e = 30$ eV in curve D. After thermal barrier formation, we let $T_e = T_i$ in curve E. The variation of f_x/f_i with ion and electron temperature accounts for both the departure from horizontal and the separation of D and E into two curves.

and no losses. The difference is that f_x/f_i in curve D is appropriate to the greater of $T_e = 30$eV or $T_e = 0.1\ T_{ic}$, and in curve E to $T_e = T_i$. Curve B shows steady-state operation with a thermal barrier providing electrostatic confinement. Curve C shows the gas fueling required if the radial diffusion losses are zero. To calculate the results in Fig. 13, we assume that the gas is deposited at the appropriate rate to refuel the plasma losses at all radii, then multiply the resulting gas current by two as discussed in Appendix A. This accounts for the excess gas that must be ionized near the plasma boundary in order to provide adequate fueling on the axis. These currents are estimated to be within a factor of about two of the actual gas-box current requirements. This uncertainty is multiplied by any uncertainty in the confinement times.

In Fig. 14, we add the currents required for buildup to the steady-state requirements and plot both the plasma density and the gas current versus time. (If the buildup rate must be very different from that used in Figs. 13 and 14, then a different gas programming will be necessary.) Two major discontinuities are seen in the gas flow requirements. The first, at the formation of the thermal barrier, may require accepting a non-ideal buildup rate during the few milliseconds that the gas-box flow is being changed, or may be handled by continuing a low-level startup gun pulse until barrier formation time, then abruptly terminating (in $<<$ 1 ms) the gun fueling. The transition to steady state will presumably be handled in a smoother way than shown here—either by a phased closing of the valves on a multivalve, nonprogrammed system, or by programming a more sophisticated system to the new flow rate.

The ion power balance in the TMX-U central cell determines the transmitter power requirements and power coupling required from the antenna to the plasma. It is given by

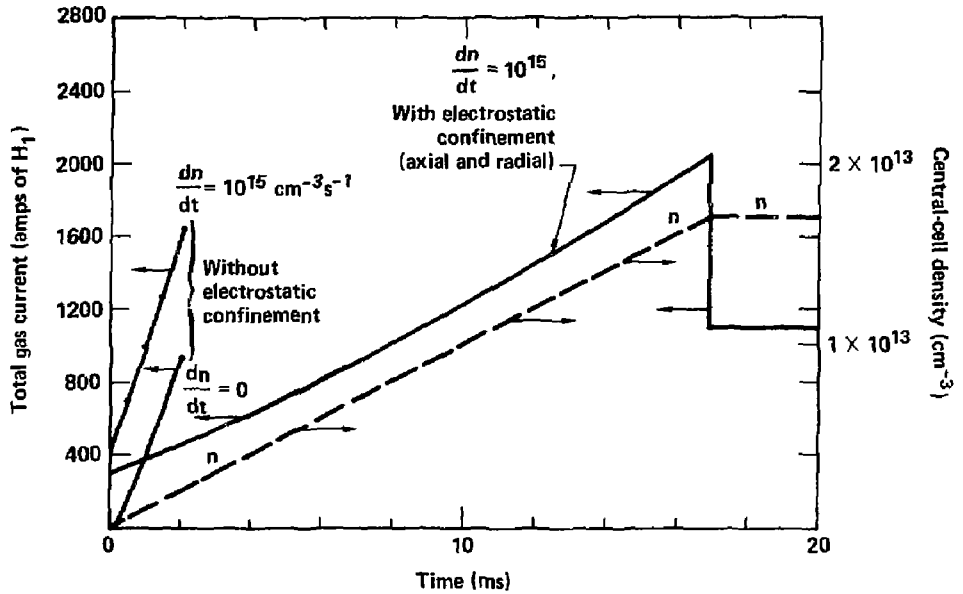

Figure 14. The required gas current, in equivalent amperes of atoms, for a linear buildup of the plasma density is shown as a function of time. The gas currents result from adding pairs of curves from Fig. 13 and shows the required flow both with and without a thermal barrier. At 17 ms, the density reaches its steady state value so the fueling can be reduced.

$$q\kappa_2 V \frac{dnE_{ic}}{dt} = 1.5 \times 10^{-8}\, n\alpha - \frac{qn_c^2\kappa_1 V\, 1.5(T_{ic} - T_{ec})}{1.6 \times 10^7\, T_{ec}^{1.5}\,(eV)} - \frac{qn_c\kappa_2 V}{\tau_{rad}}\left(1.5T_{ic} + \Gamma\frac{f_x}{f_i}\langle E_{cx}\rangle\right)$$

$$- \frac{qn_c^2 V}{n_c\tau_c}\left(\frac{\kappa_1 n\tau_1 + \kappa_2 n\tau_2}{n_c\tau_c}\right)\left\{\left[q\Phi + T_{ic}\left(\frac{n\tau_1 + 2n\tau_2}{n_c\tau_c}\right)\right] + \Gamma\frac{f_x}{f_i}\langle E_{cx}\rangle\right\} \qquad (4)$$

This equation is discussed in detail in Appendix B as Eq. B1. Briefly, the first term with $\alpha = 1$ (and implicitly $f_i = 0.4$) gives the power coupled into Phaedrus. Setting α to greater than unity provides for a more optimistic scaling, such as with the square of the radius, and to less than unity allows including additional safety factors. Values of α in the range of 1 to 4 are reasonable to expect in TMX-U. The other terms give respectively the electron drag power, radial losses, and axial losses. The charge exchange losses associated with refueling the plasma with a gas box are included as discussed in the appendices.

Before Thermal Barrier Formation

The power balance before thermal barrier formation is calculated by setting $\Phi = 0$, so that we assume the worst case of magnetic confinement only. The results of this power balance are shown in two ways. First we plot the power required to heat the central-cell ions in terms of α, the power scaling factor from Phaedrus, versus T_{ic} in Fig. 15. We conclude that a thermal barrier must be formed at densities no higher than 1 to 2×10^{12} cm^{-3} in order for ICRH to maintain T_{ic} with $\alpha < 4$ as we concluded was likely in Section 2. If we were to begin heating at higher densities, then collisional flow would prevent exceeding 50 to 100 eV ion temperatures, for α near unity. Low electron temperatures below ~30 eV can also clamp the ion temperature. If radial diffusion losses were zero as shown by the dashed lines in Fig. 16, and we

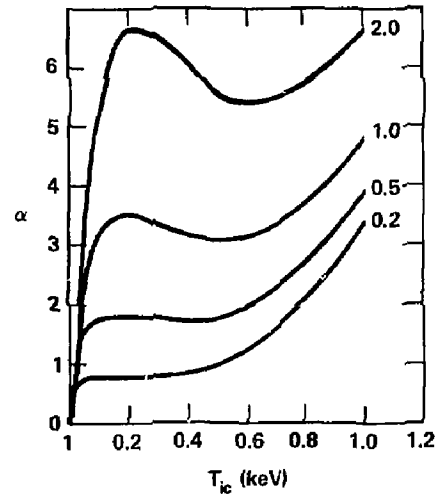

Figure 15. The ICRH power leaving the antenna, in terms of α required to heat TMX-U central-cell ions from cold to pumpable, is shown versus T_{ic} for no electrostatic axial confinement. The power requirements are shown for various densities measured in units 10^{12} cm^{-3}. The electron temperature is the greater of 30 eV or 10% of the ion temperature. We define $\alpha = 1$ at the Phaedrus operating point.

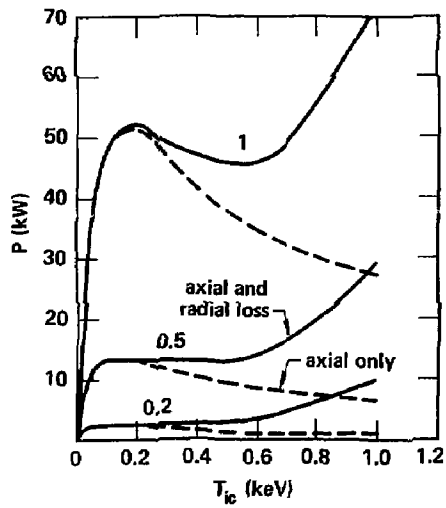

Figure 16. The ICRH power from Fig. 15 is replotted in terms of Watts. The dashed line shows the effect of zero radial diffusion. The various densities are measured in units of 10^{12} cm^{-3}.

started heating at low densities, then it would be possible to reach mirror-confined temperatures where the power loss decreased or was constant with increasing temperature. Once at high temperature, the density must then be increased slowly in order to maintain a high temperature, with limited input power and little electrostatic confinement, as must be done with ECRH in the plugs. But a better method for heating the central-cell ions is to form the thermal barrier while at low density (i.e below 10^{12} cm^{-3}). Then the density and temperature of the central-cell ions can be built-up with electrostatic (Pastukhov) confinement greatly reducing the end-loss power and consequently the ICRH power requirements. This also reduces the central-cell beta during buildup, making MHD stability easier to obtain compared with maintaining the central-cell ion temperature high enough to provide mirror confinement at densities approaching 10^{13} cm^{-3}. This approach is evaluated in the next subsection.

In order to be able to specify the requirements on a transmitter, we replot the power required in watts in Fig. 16, where the dashed line shows the power required if radial diffusion is not significant, and the solid line uses the analytic approximation for radial diffusion as in Eq. A8. From comparing Figs. 15 and 16, we conclude that about 60 kW leaving the antenna is required for this initial phase of startup.

This discussion has concentrated on ICRH at ω_{ci}; because the cold ions are then directly heated. In Fig. 17, we show some consequences of using the alternative of neutral beam heating in the central cell of TMX-U. The power required to be delivered to the cold ions was shown in Fig. 16. With neutral beam heating, the cold ions are heated by collisions with the hot ions that trapped by ionization and charge exchange. We calculate the ratio of the hot-ion to cold-ion density needed to collisionally heat the cold ions using Eq. 43 from Appendix A2 of Ref. 1. We plot the result in Fig. 17 as a function of the cold-ion density. The ratio is found to be ~15 in the startup regime before the formation of a thermal barrier. The high density of hot ions will increase the central-cell beta by the factor of more than 100 with $q\Phi/T_{ic} = 0$ and of more than 20 with $q\Phi/T_{ic} = 2.44$ as is shown in Fig. 17. This high central-cell beta makes MHD stability difficult to obtain unless the beta can be concentrated in regions of the central cell that have good curvature.[26] Low neutral-gas densities are required to allow the long charge-exchange lifetimes of greater than ~20 ms that are necessary to sustain such high hot-ion densities with ~200 A of incident neutral beam in the central cell. For these reasons, we conclude that neutral-beam heating is not optimum during startup; although some plausible scenarios have been proposed.[26]

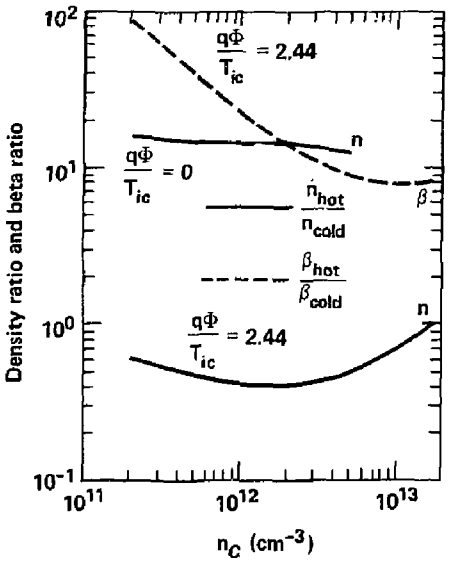

Figure 17. The ratio of hot- to cold-ion density and hot to cold beta is plotted versus the cold-ion density for collisional heating of the cold ions to a pumpable temperature with neutral beams. For all curves $dn/dt = 0$. The beta ratio curve with $\Phi = 0$ (not shown) lies above the beta curve shown by the same distance as does the density ratio.

After Thermal Barrier Formation

The power required to maintain pumpable central-cell ion temperatures against axial losses after thermal barriers have been formed is given by Eq. 4 with a suitable value for Φ. We evaluate this for $\Phi/T_{ic} = 2.44$, the same as in the design case,[1] and plot the results versus density in Fig. 18. Four curves, A-D, are shown that start with axial losses only, A, then add respectively steady-state charge exchange, radial diffusion with its associated charge exchange, and charge exchange and dE_i/dt during buildup. At design level of $n_c = 1.7 \times 10^{13}$ cm^{-3}, the axial power loss is 80 kW. Charge-exchange losses, shown in curve B, are discussed in detail in Appendices A and B. The effect of charge exchange shown in Fig. 18 curve B is roughly equivalent to dividing curve A by f_i. Radial losses, shown in curve C, are predicted to increase the power requirement by a factor of 2.6, but since radial power losses scale as $T_{ic}^{2.5}$, they should be greatly reduced below maximum energy. More accurate computations of resonant-radial-transport have been made for TMX-U and are summarized in Table V of Ref. 27. They indicate that radial losses will be less than predicted by Eq. A8, used here. The increase in charge exchange losses during buildup results from an increased gas input, beyond that required to sustain a constant density, that is required to increase the density. This last effect absorbs most of the power at low density. From comparing Figs. 16 and 17, we note that at a constant density of $n = 10^{12}$ cm^{-3}, the power required to heat the central-cell ions decreases by one to two orders of magnitude after thermal barrier formation. But, at a buildup rate of 10^{15} cm^{-3} s^{-1}, the power decreases by only a factor of one to four. The power loss through electron drag is given by the second term on the right hand side of Eq. 4, and is zero for the assumption of $T_e = T_{ic}$ used for Fig. 18.

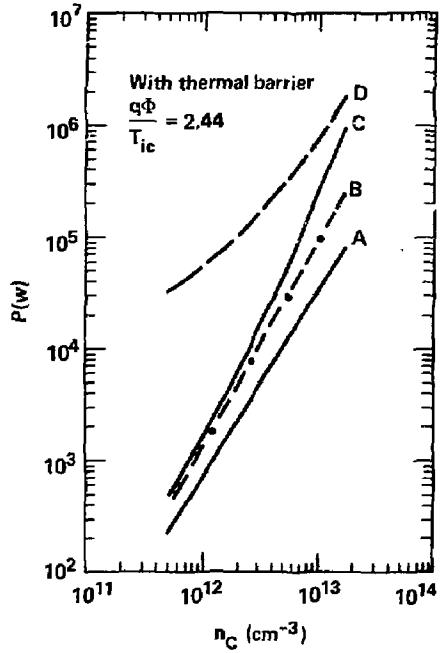

Figure 18. The power required to heat TMX-U central-cell ions to a pumpable temperature with a thermal barrier providing a confining potential $\Phi_i/T_{ic} = 2.44$ is shown versus density. The power to sustain against only axial losses in steady state is shown in curve A. In B, the power needed to sustain the plasma against the charge exchange losses associated with fueling with a gas box is added. In C, radial diffusion and the associated charge exchange is added. In D, we show the additional charge-exchange and dE_i/dt losses associated with building up the density at a rate of $dn/dt = 10^{15}$ cm^{-3} sec^{-1}.

We check the power requirements with the thermal barrier relative to the Phaedrus scaling in Fig. 19. The line is dotted above a density of 4×10^{12} cm^{-3} to indicate that this scaling cannot be expected to remain valid when the fast wave begins to propagate. We conclude that the heating should be adequate for a density buildup rate approaching 10^{15} cm^{-3} s^{-1} with a nonpropagating wave, but that a substantially faster buildup could not be heated by a single ICRH system. We have no experimental data with propagating fast waves in mirror machines from which to project power coupling and efficiencies, but we expect the heating efficiency to decrease as discussed in Section 2. However, such is not the case in tokamaks. Experiments with propagating fast waves in the PLT tokamak show that about 20% of the transmitter power is dissipated in the antenna, the remainder heats the plasma with near 100% efficiency,[8] but that efficient heating at ω_{ci} occurs only for a minority component. Similar results in mirrors could result in further applications to TMX-U as well as to MFTF-B and larger devices. Subsequent memos or reports will discuss the ICRH physics questions for mirrors, and outline experiments to study them in TMX-U.

Heating the TMX-U central-cell ions to design parameters of $T_{ic} = 900$ eV and $n_c = 1.7 \times 10^{13}$ cm^{-3} requires about 1000 kW to overcome the sum of axial losses, radial losses, and charge exchange associated with gas fueling even with a near zero buildup rate (Fig. 18). However, substantially less power, i.e., ~ 200 kW, is adequate for startup (Fig. 16) and can test the capabilities of ICRH to produce measureable heating. Since a neutral-beam system exists capable of providing several hundred kilowatts to the central-cell cold ions, it appears desirable to use ICRH for startup and initial buildup as long as it heats effectively, then continue the heating with neutral beams or with a second ICRH system operating at a higher harmonic of ω_{ci}.

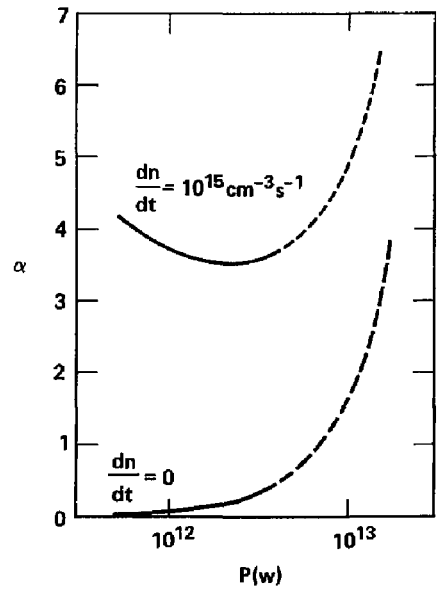

Figure 19. The power from Fig. 18 curves C and D is shown in terms of the ICRH power scaling factor α. The lines are dashed for densities greater than 4×10^{12} cm^{-3} for which the power scaling observed in Phaedrus is not considered valid.

The sensitivity of the central-cell power requirements to the confining potential $e\Phi_i/T_{ic}$ is shown in Fig. 20. This is the only figure in this report for which $e\Phi_i/T_{ic}$ is other than 0 or 2.44. Below $e\Phi_i/T_{ic} \simeq 2.5$, axial losses dominate; therefore the power requirements increase as Φ decreases. The peak in the power just above zero potential is caused by the rapid change of R_{eff} (Eq. A6) with small Φ. As explained in Appendix A, these results should be regarded with caution for $e\Phi/T_{ic}$ between 0 and 1, as these equations have not been demonstrated to be accurate in this range. Above ~2.5, axial losses decrease, but radial losses remain constant and become dominant, so the power requirement remains nearly constant. But, radial diffusion is expected to increase with $e\Phi_i$ (not included in the physics of Eq. A8), so the power requirements will probably be a minimum for some value of $e\Phi_i/T_{ic}$, increasing to either side.

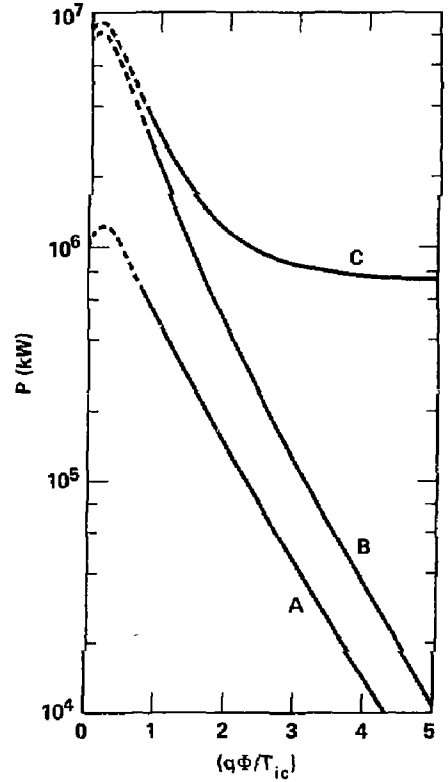

Figure 20. The steady-state power requirements from Fig. 17, A-C, are recalculated versus Φ/T_{ic}, at $n_c = 1.7 \times 10^{13}$ cm^{-3} and $T_{ic} = 900$ eV.

Conclusion

We conclude that ICRH at ω_{ci} can couple sufficient power into central-cell ions in TMX-U to satisfy the barrier pumpability constraint during startup of the thermal barriers. This conclusion is based on the measured power coupled into Phaedrus and on the calculated power requirements of TMX-U. After thermal barrier formation, ICRH at ω_{ci} can continue heating to a density of $\sim 4 \times 10^{12}$ cm^{-3}, where we expect its efficiency to decrease. Either neutral beams, or a second ICRH system operating at the second or higher harmonics, can complete heating the central-cell ions to near the design parameters.

Acknowledgments

The central cell ICRH experiments in Phaedrus were led by B. McVey with contributions by R. Breun and S. N. Golovato. J. Pew supervised the Faraday shielded antenna construction and installation and was responsible for building magnetic loop probes. A. W. Molvik thanks R. S. Post for the initial invitation to work on the Phaedrus experiment and N. Hershkowitz for a subsequent invitation and for his cooperation during that visit. F. H. Coensgen and T. C. Simonen made it possible for A. W. Molvik to work with the Phaedrus group, provided for the loan of an ICRH transmitter, and provided encouragement. Discussions with D. P. Grubb, D. L. Correll, and R. P. Drake, regarding particle and power balance calculations, were invaluable.

References

1. F. H. Coensgen, T. C. Simonen, A. K. Chargin, and B. G. Logan, *TMX Upgrade Major Project Proposal*, Lawrence Livermore National Laboratory, Livermore, CA, LLL-PROP-172 (1980).
2. D. K. Smith, *Fundamental Resonance Ion Cyclotron Heating in the Phaedrus End Plugs*, Ph.D. Thesis, University of Wisconsin, (August, 1980), pgs. 23 and ff.
3. B. McVey, et al., *Ion Cyclotron Resonance Heating Studies in the Central Cell of the Phaedrus Tandem Mirror*, to be published.
4. Mirror physics staff, Thermal Barrier Startup Meetings, (1981).
5. S. Suckewer, et al., "Radiation Losses in PLT During Neutral-Beam and ICRF Heatin Experiments," *Nuc. Fusion* **21**, 981 (1981).
6. R. C. Isler, et al., "Influence of Neutral-Beam Injection on Impurity Transport in the ISX-B Tokamak," *Phys. Rev. Lett.* **47**, 649 (1981).
7. A W. Molvik, "Operating Windo\ for Startup of Thermal Barrier in TMX-U," Lawrence Livermore National Laboratory, Livermore, CA, Memo, Feb., 1981.
8. J. Hosea, et al., *Fast Wave Ion Cyclotron Heating in the Princeton Large Torus*, Plasma Physics Laboratory, Princeton, NJ, PPPL-1729 (1981), and P. L. Colestock, S. L. Davis, J. C. Hosea, D. Q. Hwang, and H. R. Thompson, *Modeling Of ICRF Heating in PLT*, PPPL-1754 (1981).
9. F. W. Baity, Jr., D. L. Hillis, J. C. Glowienka, "Enhancement of EBT Ring Parameters During Ion Cyclotron Heating," in *Proceedings of the Second EBT Ring Physics Workshop* (1981), paper E.8.
10. A. W. Molvik, et al., *Initial TMX Central-Cell ICRH Experiments*, Lawrence Livermore Laboratory, Livermore, CA, UCID-18866 (1980).
11. R. Breun, et al., "Initial Results from the Tandem Mirror, Phaedrus," in *Proceedings of the Eighth International Conference on Plasma Physics and Controlled Nuclear Fusion Research*, Brussels, 1980 (IAEA, Vienna, 1981), Vol. 1, P. 105.
12. R. Breun, et al., "Experiments in a Tandem Mirror Sustained and Heated Solely by rf", *Phys. Rev. Lett.* **47**, 1835 (1981).
13. J. C. Hosea and R. M. Sinclair, "Ion Cyclotron Wave Generation in the Model C Stellarator," *Phys. Fluids* **13**, 701 (1970).
14. Miklos Porkolab, *Review of rf Heating*, International School of Plasma Physics, Varenna, Italy, Sept. 1-10, 1977. Preprint PFC/JA-70-3.
15. R. L. Freeman and E. M. Jones, "Atomic Collision Processes in Plasma Physics Experiments", Culham Laboratory Report CLM-R 137 (1971?).

16. R. A. Breun, University of Wisconsin, Private communication (1981).
17. A. W. Molvik, R. A. Breun, S. N. Golovato, N. Hershkowitz, B.McVey, D. Smatlak, and L. Yujiri, "Observation of Macroscopic Stability Limits in a Tandem Mirror," *Phys. Rev. Lett.* **48**, 742 (1982).
18. T. Watari, et al., "Radio-Frequency Plugging of a High Density Plasma," *Phys. Fluids* **21**, 2076 (1978).
19. O. M. Shvets, S. S. Kalinichenko, A. I. Lysoivan, N. I. Nazarov, A. S. Slavnyi, and V. F. Tarasenko, "Experimental Excitation of Ion Cyclotron Waves With a Slot Antenna," *Sov. J. Plasma Phys.* **7**, 261 (1981).
20. D. Q. Hwang, et al., *Fast Wave Heating in the Two Ion Hybrid Regime on PLT*, Plasma Physics Laboratory, Princeton University, Princeton, NJ, PPPL-1676 (1981).
21. S. Iizuka, et al., "Propagation and Absorption of the Fast Magnetosonic Wave in the Ion-Cyclotron Range of Frequencies in the DIVA Tokamak," *Phys. Rev. Lett.* 45, 1256 (1980).
22. J. E. Scharer, F. D. McVey, and T. K. Mau, "Fast-Wave Ion-Cyclotron and First-Harmonic Heating of Large Tokamaks," *Nuc. Fusion* **17**, 297, (1977).
23. Y. Amagishi, A. Tsushima, and M. Inutake, "Conversion of Compressional Alfvén Waves into Ion-Cyclotron Waves in Inhomogeneous Magnetic Fields," *Phys. Rev. Lett.* 48, 1183 (1982).
24. O. Eldridge, "Electron Cyclotron Heating as Resonant Diffusion", *Phys. Fluids* 15, 676 (1972).
25. L. L. Lao, et al., "Spatial Structure of the SM-1 Symmetric Mirror Hot Electron Ring Using Diamagnetic Measurements," in *Proceedings of the Second EBT Ring Physics Workshop* paper D.9. (1981).
26. D. P. Grubb in *Negative Potential Operation of TMX-U*, P. Paulsen, et al., Appendix A, Report UCID-19341, Lawrence Livermore National Laboratory, Livermore, CA (April 1982).
27. J. H. Foote, A. K. Chargin, R. H. Cohen, T. B. Kaiser, C. V. Karmendy, T. C. Simonen, R. L. Wong, *TMX Upgrade Magnet System—Design Characteristics and Physics Considerations*, UCRL-86677 Lawrence Livermore National Laboratory, Livermore, CA, (1981). Catalogue of ~100 codes available from Carol Tull or Susarla Murty.
A1. G. E. Gryczkowski, CSCC1A code, and related codes, MFECC, Lawrence Livermore National Laboratory, Livermore, CA (1980), (contact Carol Tull or Susarla Murty, LLNL).
A2. E. B. Hooper, G. E. Gryczkowski, and R. P. Drake, "Lebers Plasma Generation in Gas Box Fueling for Tandem Mirrors," Report UCRL-86271, Sept. 1981, to be published.
A3. R. P. Drake, et al., in UCRL-53120, pgs. 9-10 through 9-11.
A4. D. P. Grubb, Private communication, Lawrence Livermore National Laboratory, Livermore, CA (1982).
A5. T. D. Rognlien and T. A. Cutler, "Transition from Pastukhov to Collisional Confinement in a Magnetic and Electrostatic Well," *Nucl. Fusion* **20**, 1003 (1980).
A6. R. H. Cohen, M. E. Rensink, T. A. Cutler, and A. A. Mirin, "Collisional Loss of Electrostatically Confined Species in a Magnetic Mirror," *Nucl. Fusion* **18**, 1229 (1978).
A7. T. D. Rognlien and T. A. Brengle, "Warm Plasma Axial Flow Through a Magnetic Mirror," *Phys. Fluids* **24**, 871 (1981).
A8. D. Correll, "Changes to GFITS Program," Memo, May, 1980.
A9. R. P. Drake in *Summary of Results from the Tandem Mirror Experiment (TMX)* ed. T. C. Simonen, Appendix C, Report UCRL-53120, Lawrence Livermore National Laboratory, Livermore, CA (Feb., 1981).
A10. D. Correll, "TMX-U Generalized Formula for Pastukhov Losses," Memo Jan., 1982.
A11. C. V. Karmendy, "Effective Lengths (for volume calculations) in TMX-Upgrade," Lawrence Livermore National Laboratory, Livermore, CA, Memo, Jan., 1981.

Appendix A
Central Cell Ion Particle Balance

We calculate the gas fueling requirements for TMX-U based on the computed losses of ions, on the ionization efficiency, and on the relative amounts of gas absorbed by the plasma to that pumped by the walls. Our results differ from previous estimates of gas fueling in the following: The ionization efficiency is 4.6^{-1} rather than 2^{-1} as was appropriate to TMX. We assume a gas utilization efficiency of 2^{-1}, based on TMX measurements, which we multiply by the ionization efficiency. We include the amount of gas necessary to build-up the plasma density in addition to the steady-state requirements.

$$\frac{dn_c\kappa_2 V}{dt} = \frac{f_i J_{gas}}{\Gamma} - \frac{qn_c\kappa_2 V}{\tau_{rad}} - \frac{qn_c^2 V}{n_c\tau_c}\left(\frac{\kappa_1 n\tau_1 + \kappa_2 n\tau_2}{n_c\tau_c}\right) \tag{A1}$$

where the terms are defined as follows: the ionization efficiency f_i is

$$f_i = \frac{\langle\sigma v\rangle_i + \langle\sigma v\rangle_e}{\langle\sigma v\rangle_i + \langle\sigma v\rangle_e + \langle\sigma v\rangle_x} \tag{A2}$$

The rates, $\langle\sigma v\rangle$, are averaged over Maxwellian distributions.[15] The results are displayed in Fig. 6(a) for plasma interactions with atoms and in Fig. 6(b) for interactions with molecules. The results are shown in terms of f_x/f_i versus T_{ic}, where $f_x = (1 - f_i)$. The three curves are for $T_e = 30$ eV and $T_e = 0.1\ T_{ic}$ which are appropriated before thermal barrier formation, and for $T_e = T_{ic}$ which is appropriate after barrier formation.

We have considered only atomic charge exchange in our analytic expressions for fueling and power requirements in this report. Molecular charge exchange is included by normalizing our results to TMX, and to codes that include both atomic and molecular interactions. We compute gas penetration and ionization rates for gas puffing around a cylindrical plasma using the CSCC1A code.[A1] This is appropriate to densities below 10^{12} cm^{-3}, where substantial gas leakage around the jaws of a gas box can be expected. The density of molecules, Franck-Condons, and energetic charge exchange neutrals are shown versus radius in Fig. A-1. We observe that the density of atoms is nearly independent of radius; therefore, the charge exchange model of Eq. (1) is quite accurate in taking the charge exchange to be proportional to the plasma density. We can ignore molecular charge-exchange as long as $T_{ic} << 1000$ eV [compare Figs. 6(a) and 6(b)], or the plasma density $n >> 10^{12}$ cm^{-3} so that H_2 molecules do not penetrate far into the plasma. One or both of these conditions is satisfied for every case evaluated here.

Calculating the gas fueling requirements with $\Gamma = 1$ would be equivalent to assuming that the gas was ionized where it was needed to sustain against losses. However, we know that the gas density, and hence the ionization rate, is higher at large radii, whereas the losses are greater at small radii. Evaluation of gas box fueling for TMX[A2,A3] found that gas penetration into a slab model plasma fan, even at high densities, was similar to the case shown in Fig. 2. These code runs showed that the gas current requirements are about twice that calculated from Eq. (1), with a factor of two uncertainty.

Measurements[A4] of the plasma loss currents and the gas fueling current in TMX are listed in the last column of Table A-1. These measurements imply a gas box efficiency of 2.3^{-1}, consistent with the value of $\Gamma = 2$ found above. The value of Γ depends on the gas reflectivity of the wall: if the reflectivity were 100%, then Γ would be unity, and dividing by the ionization efficiency would result in an overestimate of the fueling requirements. The calculation as summarized in Table A-1 is correct if the charge exchange neutrals have a high sticking coefficient, and thermal gas and Franck-Condons have sticking coefficients similar to in TMX. All results shown in this report assume a gas input of $\Gamma = 2$.

The axial confinement time is described in terms of long mean free path confinement, $n\tau_1$ and short mean free path confinement, $n\tau_2$, as follows[A5]:

$$n_c\tau_c = n\tau_1 + n\tau_2 \tag{A3}$$

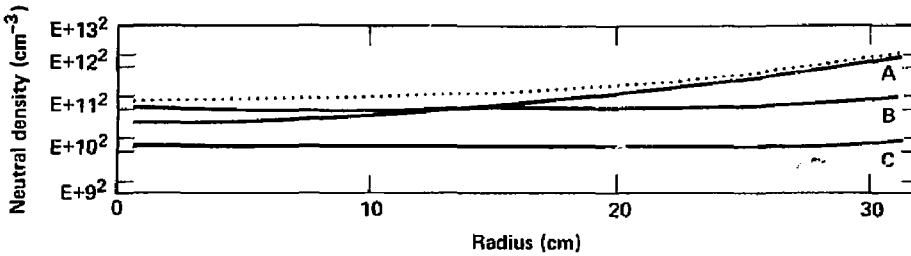

Figure A-1. The computed neutral density within the plasma due to gas puffing is plotted versus radius for (a) H_2 molecules, (b) Franck-Condons of 2 eV energy, and (c) energetic charge exchange atoms from the hot plasma. The plasma density profile is parabolic, peaking at $n = 5 \times 10^{11}$ cm^{-3} and reaching zero at r = 32 cm. The ion and electron temperature profiles are also parabolic, peaking at 90 eV and 30 eV respectively, and reaching zero at r = 40 cm.

$$n\tau_1 = 5.47 \times 10^5 A^{0.5}\,(\mathrm{AMU})\, T_{ic}^{1.5}(\mathrm{eV})\, \frac{R_{eff}}{R_{eff}}\, \ln(2R_{eff} + 2)\, \frac{1 + \frac{1}{4X}}{1 + \frac{1}{2X}} \times \exp(X) \qquad \text{(A4)}$$

and the collisional confinement term is derived from Rognlien and Cutler[A5]

$$n\tau_2 = 1.28 \times 10^{-6}\, n_e\,(\mathrm{cm}^{-3})\, L_c\,(\mathrm{cm})\, R_{eff} A^{0.5}\,(\mathrm{AMU})\, T_{ic}^{-0.5}\,(\mathrm{eV})\, \exp(X). \qquad \text{(A5)}$$

where we use the equation for Pastukhov confinement derived from R. Cohen, et al.[A6], and explicitly write G(R) and I(1/X) in terms of R_{eff} and X, both of which are defined below. The form used for $n\tau$ goes smoothly to the limit of magnetic confinement for $\Phi = 0$[A7,A8] as discussed below and to the limit of Pastukhov confinement for $\Phi > 1$.[A5,A6,A9,A10] These equations are at present the most accurate analytic forms available for $n\tau$. Correll has estimated the error in $n\tau_1$ to be less than 20%.[A10] Rognlien and Brengle[A7] have shown that $n\tau_2$ can differ by factors of several from Eq. (5) when $T_e > T_i$. But, in this report, $n\tau_2 > n\tau_1$ only at low T_{ic} and low Φ for which $T_e << T_{ic}$; consequently, the error in Eq. (A5) is believed to be small. Although these equations are correct at the limits of Φ either zero or larger than one, and connect smoothly between the limits, their predictions in the vicinity of $\Phi = 1$ have not been checked so should not be relied on there.

Table A-1. Comparison of Calculated Gas Fueling Requirements for TMX-Upgrade and Measured Fueling in TMX.

	TMX-U	TMX*
n_e(cm^{-3})	1.7×10^{13}	
$l_{\parallel}$(A)	26	150
$l_{\perp}$(A)	94	150
l_{pump}(A)	0	-
l_{cc}(CX on Beam)(A)	-	-
Total Losses(A)	120	300
$\frac{1}{f_i} = \frac{\Sigma\langle\sigma v\rangle}{\langle\sigma v\rangle}$	4.6	2.3
[Gas Box Eff.]$^{-1}$	2	(computed) 2.3
Total Atom Current (A)	1100	(Measured) 1580

*See Ref. A4.

The effective mirror ratio R_{eff} is given in terms of the mirror ratios R_c from the central cell and R_p from the potential peak in the plugs. This was derived by Drake[A9] for the collisional limit. We apply it also to the long mean free path limit, arguing that any error involved is small, because it essentially appears only in a logarithic term.

$$R_{eff} = \frac{R_c}{R_p}\left\{1 - \left(1 - \frac{1}{R_p}\right)\exp\frac{-2q\Phi_c}{T_{ic}(R_p - 1)}\right\}^{-1} \tag{A6}$$

and we define

$$X = q\Phi/T_{ic}.$$

Other effects, that are not included in the results in this report, are due to the pump beams.[A10] Central cell ions are lost by charge exchange of passing ions on the pump beams, but can also be refueled from electrostatic trapping of half and third energy pump beam atoms that are ionized or charge exchanged at the bottom of the barrier potential well. This effect can be written[A4]

$$\frac{dn\kappa_2 V}{dt} = 2I_b^p f_{cx}^p (1 - f_{circ})\frac{g(b)n_{poss}}{n_{total}} \tag{A7}$$

where f_{circ}, the fraction of the pump beams interacting at the bottom of the barrier, is much less than one. The upper limit is evaluated to be 60 A, using values from Table A-1 of Ref. 12. This term is seen to be small during buildup (compare 60 A with the fueling rates shown in Fig. 2) and when Φ is below design level, but may be a significant correction during steady state, particularly if radial diffusion is smaller than assumed here.

In the limit of $\Phi = 0$, $R_{eff} \to R_c$, and we obtain the magnetic confinement times that were used to determine the degree of electrostatic enhancement of observed TMX confinement times:[A7,A8]

$$n\tau_l = n\tau_{ii}\log(R_c)$$

where $n\tau_{ii}$ is the ion-ion scattering time, and

$$n\tau_z = nL(\pi m_i/2T_{ic})^{0.5}R_c$$

where m_i is the ion mass.

We include the effects of radial diffusion using an approximate scaling law (Eq. (1) from Appendix A2 of Ref. 1)

$$\tau_{rad}(\text{sec}) = 632\ A^{-0.5}\ T_{ic}^{1.5}(\text{eV}). \tag{A8}$$

This overestimates radial losses by a factor of about 2, based on recent computations by R. Cohen.[27]

We effectively average over a parabolic density profile, that goes to zero at r = 32 cm, by using the constants $\kappa_1 = 0.33$ for a loss proportional to n_c^2 and $\kappa_2 = 0.5$ for a loss proportional to n_c, as in Ref. 1, Appendix A2. We average κ_1 and κ_2 in the same way as Rognlien and Cutler[A5] averaged the axial loss energy. We take the length to be 508 cm.[A11] All operation is assumed to be with hydrogen, so A = 1.

In Fig. 13 we show the gas feed requirements for no electrostatic confinement, $\Phi = 0$, as well as the gas feed requirements for thermal barriers providing electrostatic axial confinement with $q\Phi/T_{ic} = 2.44$. For the latter case, line c shows the gas requirements if radial diffusion is negligible. The ion temperature is given by

$$T_{ic} = \left(\frac{n_c}{6.3 \times 10^8}\right)^{.67}$$

and is near the minimum for pumpability. During the density buildup, an additional current is required. Letting the axial and radial loss terms be zero in Eq. (1), we obtain

$$I(A) = \frac{q\kappa_2 V\Gamma}{f_i}\frac{dn}{dt} = \frac{1.3 \times 10^{-13}\Gamma}{f_i}\frac{dn}{dt} \tag{A9}$$

which is shown in Fig. 13 for $dn/dt = 10^{15}$ cm^{-3} s^{-1}, corresponding to a build-up time of 17 ms, and requiring a total gas input of 260 (amps H_1)/f_i for $\Gamma = 2$.

In Fig. 14 we add the currents required for buildup to the steady state requirements and plot both the plasma density and the gas current versus time. (If the buildup rate must be very different from 10^{15} cm^{-3} s^{-1}, then a different gas programming will be necessary.) Two major discontinuities are seen in the gas flow requirements. The first, at the formation of the thermal barrier, may require accepting a non-ideal buildup rate during the few milliseconds that the gas box flow is being changed, or may be handled by continuing a low level startup gun pulse until barrier formation time, then abruptly terminating (in $<<$ 1 ms) the gun fueling. The transition to steady state will presumably be handled in a smoother way than shown here: either by a phased closing of the valves on a multivalve, nonprogrammed system, or by programming a more sophisticated system to the new flow rate.

BS/km

Appendix B
Power Balance with and without Electrostatic Confinement

The general power balance for ions is similar to the particle balance of Eq. A1 with the addition of electron drag. The power balance is given by

$$q\kappa_2 V \frac{dnE_{ic}}{dt} = 1.5 \times 10^{-8}\, n_c \alpha - \frac{qn_c^2 \kappa_1 V\, 1.5(T_{ic} - T_{ec})}{n\tau_d}$$

$$- \frac{qn_c \kappa_2 V}{\tau_{rad}} \left(1.5\, T_{ic} + \Gamma \frac{f_x}{f_1} (E_{cx}) \right)$$

$$- \frac{qn_c^2 V}{n_c \tau_c} \left(\frac{\kappa_1 n\tau_1 + \kappa_2 n\tau_2}{n_c \tau_c} \right) \left\{ \left[q\Phi + T_{ic} \left(\frac{n\tau_1 + 2n\tau_2}{n_c \tau_c} \right) \right] + \Gamma \frac{f_x}{f_1} (E_{cx}) \right\} \qquad \text{(B1)}$$

where $n_c\tau_c$ is given by Eqs. A3–5. In this report, we have taken Φ to be zero in the fourth term for magnetic confinement without a thermal barrier. The individual terms are as follows: The first term with $\alpha = 1$ (and implicitly $f_i = 0.4$) gives the power coupled into Phaedrus. Setting α to greater than unity provides for a more optimistic scaling, such as with the square of the radius, and to less than unity allows including additional safety factors. Values of α in the range of 0.5 to 4 are reasonable to expect in TMX-U. The electron drag time, for the second term on the right hand side of Eq. 12, is given by

$$n\tau_d = 1.6 \times 10^7\, T_{ec}^{1.5}\ (\text{eV}) \qquad \text{(B2)}$$

With thermal barriers, we assume that $T_{ic} = T_{ec}$, resulting in zero power exchange from the drag term. But without thermal barriers, we assume that T_e is the greater of 0.1 T_{ic} or 30 eV; then electron drag is significant. The third term gives the radial diffusion power loss for an average energy loss of 1.5 T_{ic} and a lifetime given by Eq. A8. In the fourth term of Eq. B1, the axial loss time constant is given by Eqs. A3–5 of Appendix A. The average energy per ion lost axially is weighted by T_{ic} for τ_1 and $2T_{ic}$ for τ_2.[A5] In evaluating the power requirements without thermal barriers, we have assumed $T_{ic} >> q\Phi$.

The power loss due to the fraction of gas that is charge exchanged, rather than ionized, is included in the third and fourth terms in the f_x/f_i term. The factor Γ allows varying the amount of gas injection from $\Gamma = 1$, which provides exactly enough gas to sustain the plasma density against axial and radial losses. During steady state $\Gamma = 2$, as discussed in Appendix A, gives our best estimate of the gas fueling required. Increasing Γ to greater than two provides the extra gas required during density buildup as discussed in Appendix A, and shown in Fig. 13. This increased gas input increases the power loss from charge exchange shown in curve D of Fig. 18. The average energy of a charge exchanged ion is estimated from computations as follows[26]: A gas penetration code[A1] computes the current and power lost from the central cell due to charge exchange on the amount of gas needed to sustain the plasma core by ionization. The average energy of a charge exchange neutral is then computed to be

$$\langle E_{cx} \rangle = \frac{\text{Charge exchange power}}{(\textit{Ion loss current})\,(f_x/f_i)} \qquad \text{(B3)}$$

The average energy of a charge exchange neutral corresponds to about T_{ic} at the core or about twice the temperature at the edge for the parabolic temperature profiles used here. So, for all results shown in this report, we use a gas input rate $\Gamma = 2$ and a charge exchange energy of $\langle E_{cx} \rangle \approx T_{ic}$. While this is our best estimate for TMX-U, we note that a combination of measured loss currents and computed charge exchange power losses in TMX indicated that $\langle E_{cx} \rangle \simeq 0.25\ T_{ic}$.[A4]

Two effects are neglected in this report. The first is the conversion of electrostatic potential energy to kinetic energy by radially diffusing ions, which could be included by increasing the coefficient on the average energy of radially diffusing ions to greater than 1.5 T_{ic}. The second effect is due to the pump beams,[26] as discussed in Appendix A. The power loss from the central cell is

$$P_{pump} = 2I_p f_{cx}^p \frac{g(b)\, n_{pass}}{n_{total}} \left(1.5\, T_{ic} - f_{circ} \langle E_{circ} \rangle \right)$$

This effect will initially be an energy drain on the central cell-ions until the potential becomes large enough that f_{circ} becomes nonzero. Then the terms in parenthesis will tend to cancel. When $f_{circ} = 0$, the maximum value of this term, again using data from Table A-1 of Ref. 1, is $P_{pump} \simeq (n_p/7 \times 10^{12})$ 50 kW, which will be small except near design level, where it could approach the axial power loss rate.

The power balance depends on the average energy of charge exchange neutrals, the radial diffusion lifetime, the value of the confining potential that provides axial confinement, and the gas fueling rate required to sustain and buildup the plasma. The latter has been measured in TMX and found to fit gas penetration code predictions,[42] but is sensitive to the actual density and temperature profiles. The first two effects have not been experimentally determined; factors of two uncertainty in these quantities are possible. Axial confinement in TMX was accurately modeled by the equations used here. Overall, a factor of two uncertainty can be expected in the power balance calculations.